

Analysis of Incident-Photon-Energy and Polarization Dependent Resonant Inelastic X-Ray Scattering from La_2CuO_4

Manabu Takahashi ¹ * , Junichi Igarashi ² and Takuji Nomura ³

¹*Faculty of Engineering, Gunma University, Kiryu, Gunma 376-8515*

²*Faculty of Science, Ibaraki University, Mito, Ibaraki 310-8512*

³*Synchrotron Radiation Research Center, Japan Atomic energy Agency, Hyogo 679-5148*

We present a detailed analysis of the incident-photon-energy and polarization dependences of the resonant inelastic x-ray scattering (RIXS) spectra at the Cu K edge in La_2CuO_4 . Our analysis is based on the formula developed by Nomura and Igarashi, which describes the spectra by a product of an incident-photon-dependent factor and a density-density correlation function for $3d$ states. We calculate the former factor using the $4p$ density of states from an ab initio band structure calculation and the latter using a multiorbital tight-binding model within the Hartree-Fock approximation and the random phase approximation. We obtain spectra with rich structures in the energy-loss range 2-5 eV, which vary with varying momentum and incident-photon energy, in semi-quantitative agreement with recent experiments. We clarify the origin of such changes as a combined effect of the incident-photon-dependent factor and the density-density correlation function.

KEYWORDS: La_2CuO_4 , RIXS, XES, tight-binding model, theory

1. Introduction

Taking advantage of strong synchrotron light sources, the resonant inelastic x-ray scattering (RIXS) has recently become a powerful tool to probe charge excitations in solids. K -edge resonances are widely used in transition-metal compounds, because it could detect momentum dependence of charge excitations.¹⁻¹⁶ It is described as a second-order optical process that a $1s$ -core electron excites to an empty $4p$ state with absorbing a photon, then charge excitations are created in the $3d$ states to screen the core-hole potential, and finally the photoexcited $4p$ electron recombines with the $1s$ -core hole with emitting a photon. In the end, the charge excitations are left with carrying the energy and the momentum transferred from photon.

Intensive studies have been carried out on Cu oxide perovskite compounds for better understanding of the unconventional high- T_C superconductivity.^{3-5,7-16} In the undoped material La_2CuO_4 , the spectra are found to be composed of several peaks which changes with changing momentum transfer.^{5,13} Such spectra have been theoretically studied by several groups.¹⁷⁻²² Nomura and Igarashi (NI)^{19,20} have proposed a general formalism of the RIXS spectra by

*mtakahas@phys.sci.gunma-u.ac.jp

extending the resonant Raman theory developed by Nozières and Abrahams²³ on the basis of the many-body formalism of Keldysh. The NI formula makes it possible to calculate the RIXS spectra on complicated models including many orbitals, and provides clear physical interpretations to the RIXS spectra. It is composed of two factors, one describing an incident-photon dependence and the other the density-density correlation function for the $3d$ states. Similar formulas which are proportional to the density-density correlation function have been derived by using different methods.²⁴

This formula has been applied to a two-dimensional cuprate La_2CuO_4 ²⁰ and quasi-one-dimensional cuprates SrCuO_3 ¹⁹ and CuGeO_3 .⁹ In these studies, the electronic structures have been calculated on the d - p model within the Hartree-Fock approximation (HFA) in the antiferromagnetic (AFM) phase. It is known that the HFA works well to describe electronic structures in the AFM insulators. Two-particle correlations have been taken into account within the random phase approximation (RPA). The calculated spectra as a function of energy loss have reproduced well the RIXS spectra varying with varying momentum. The RIXS spectra have been interpreted as a band-to-band transition. The RPA correlation had to be included for obtaining better agreement with the experiment.

Subsequently, the present authors have analyzed multiple-scattering contributions due to the core-hole potential, because the core-hole potential is not definitely weak.²² Having evaluated the multiple-scattering contributions by means of the time-representation method by Nozières and De Dominicis,²⁵ we have found that main contributions could be absorbed into the shift of the core-level energy with minor effects on the RIXS spectral shape. This result partly justifies the use of the Born approximation. Quite recently, we have demonstrated the usefulness of the NI formula by analyzing the RIXS spectra in NiO .²⁶ Using the HFA and the RPA on the multiorbital tight-binding model, we have obtained the RIXS spectra, which vary with varying momentum, in quantitative agreement with the experiment.²⁷

Recently, Lu et al.¹³ have presented comprehensive RIXS data with systematically changing the incident-photon energy in La_2CuO_4 . Kim et al.¹⁴ have recounted the momentum transfer dependence and incident photon polarization dependence of the RIXS line shape in a number of cuprates. Ellis et al.¹⁵ have reported the high resolution RIXS spectra in La_2CuO_4 . Their data show fine structures as a function of energy loss, in addition to the peaks found in previous data, which vary with varying the incident-photon energy. Although our previous analysis using the d - p model has been successful to clarify the origin of the RIXS spectra,²⁰ the analyses have been limited to the situation of the incident-photon energy corresponding to the excitation of the $1s$ electron to the peak of the $4p$ density of states (DOS). Also, it seems hard to explain the newly observed fine structures. Encouraged by the success in the application to NiO ,²⁶ we extend the d - p model to a multiorbital tight-binding model, which includes all O $2p$ and Cu $3d$ orbitals as well as the full intra-atomic Coulomb interaction

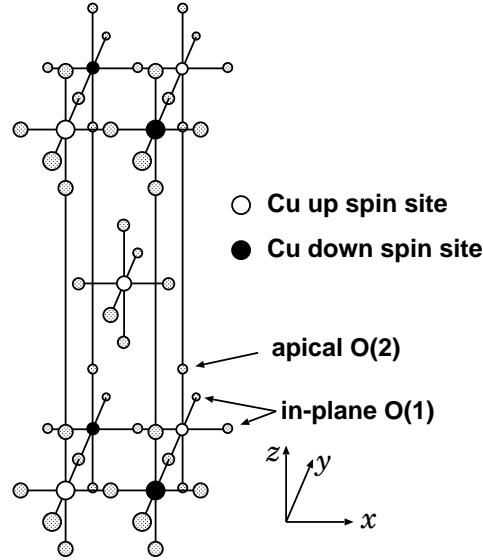


Fig. 1. Sketch of the assumed crystal and magnetic structure of La_2CuO_4 with omitting La sites. The tiny tilting, rotation and the Jahn-Teller distortion of CuO_6 octahedron are neglected.

between $3d$ orbitals, and analyze the incident-photon-energy and polarization dependences of the RIXS spectra in comparison with the experiment.^{13,15}

In the present study, we obtain the AFM insulating solution having an energy gap ~ 1.7 eV within the HFA. Note that the band structure calculation with the local density approximation (LDA) fails to reproduce the insulating state. These energy bands by the HFA are used to calculate the density-density correlation function. We treat the two-particle correlations within the RPA. The incident-photon-dependent factor is calculated by using the $4p$ DOS obtained from the ab-initio band structure calculation. We obtain richer structures in RIXS spectra in a range of energy loss $2 \sim 5$ eV than those obtained by the d - p model analysis,²⁰ which vary with varying momentum transfer and incident-photon energy. The obtained spectra are in semi-quantitative agreement with the experiments.¹³⁻¹⁵ We clarify the origin of such spectral change as a combined effect of the incident-photon-dependent factor and the density-density correlation function.

The present paper is organized as follows. In Sec. 2.1, we introduce the multiorbital tight-binding model. In Sec. 2.2 we discuss the electronic structure within the HFA in the AFM phase of La_2CuO_4 . In Sec. 3, we briefly summarize the NI formula for the RIXS spectra. In Sec. 4, we present the calculated RIXS spectra in comparison with the experiment. The last section is devoted to the concluding remarks.

2. Electronic Structure of La_2CuO_4

2.1 Multiorbital tight binding model

For explaining the fine structures in the observed RIXS spectra, we need to extend a simple d - p model to a multiorbital tight-binding model, in which most of parameters are determined from an ab-initio band structure calculation.

As shown in Fig. 1, we approximate the crystal structure of La_2CuO_4 by a simple tetragonal one without the Jahn-Teller distortion and the tilt of the CuO_6 octahedron. Extending the d - p model, we introduce a tight-binding model involving all Cu $3d$ orbitals and O $2p$ orbitals at the in-plane and apical sites. We exclude orbitals belonging to the La atoms, since those orbitals play minor roles in the electronic states near the insulating gap.²⁸ Thereby the Hamiltonian may be written as

$$H = H_0 + H_I, \quad (1)$$

$$H_0 = \sum_{im\sigma} E_{im\sigma}^d n_{im\sigma}^d + \sum_{jm\sigma} E_{jm\sigma}^p n_{jm\sigma}^p + \sum_{\langle i,j \rangle} \sum_{\sigma mm'} \left(t_{im,jm'}^{dp} d_{im\sigma}^\dagger p_{jm'\sigma} + \text{H.c.} \right) \\ + \sum_{\langle j,j' \rangle} \sum_{\sigma mm'} \left(t_{jm,j'm'}^{pp} p_{jm\sigma}^\dagger p_{j'm'\sigma} + \text{H.c.} \right) + \sum_{\langle i,i' \rangle} \sum_{\sigma mm'} \left(t_{im,i'm'}^{dd} d_{im\sigma}^\dagger d_{i'm'\sigma} + \text{H.c.} \right), \quad (2)$$

$$H_I = \frac{1}{2} \sum_i \sum_{m_1\sigma_1} \sum_{m_2\sigma_2} \sum_{m_3\sigma_3} \sum_{m_4\sigma_4} g(m_1\sigma_1 m_2\sigma_2; m_3\sigma_3 m_4\sigma_4) d_{im_1\sigma_1}^\dagger d_{im_2\sigma_2}^\dagger d_{im_4\sigma_4} d_{im_3\sigma_3}. \quad (3)$$

The part H_0 represents the kinetic energy, where $d_{im\sigma}$ and $p_{jm\sigma}$ denote the annihilation operators of an electron with spin σ in the $3d$ orbital m at Cu site i and that of an electron with spin σ in the $2p$ orbital m at the O site j , respectively. Number operators $n_{im\sigma}^d$ and $n_{jm\sigma}^p$ are defined as $n_{im\sigma}^d = d_{im\sigma}^\dagger d_{im\sigma}$, $n_{jm\sigma}^p = p_{jm\sigma}^\dagger p_{jm\sigma}$. The transfer integrals, $t_{im,jm'}^{dp}$, $t_{jm,j'm'}^{pp}$, and $t_{im,i'm'}^{dd}$ are evaluated from the Slater-Koster (SK) two-center integrals, $(pd\sigma)$, $(pd\pi)$, $(pp\sigma)$, $(pp\pi)$, $(dd\sigma)$, $(dd\pi)$, $(dd\delta)$.²⁹ We use the SK parameters determined by the ab-initio band structure calculation.²⁸ The part H_I represents the intra-atomic Coulomb interaction on Cu sites. The interaction matrix element $g(\nu_1\nu_2; \nu_3\nu_4)$ (ν stands for spin-orbit($m\sigma$)) is written in terms of the Slater integrals F^0 , F^2 , and F^4 . Among them, F^2 and F^4 , which are known to be slightly screened by solid-state effects, are taken from the cluster model exact diagonalization analysis of the X-ray photoemission spectroscopy.³⁰ On the other hand, F^0 is known to be considerably screened, so that we regard the value as an adjustable parameter. The Coulomb interaction on O sites is absorbed into a renormalization of the O $2p$ level parameters $E_{jm\sigma}^p$. The d -level position relative to the p -levels is given by the charge-transfer energy Δ defined as $\Delta = E_{e_g} - E_p + 9U$ in the d^9 configuration.³¹ Here U is the multiplet-averaged d - d Coulomb interaction given by $U = F^0 - (2/63)F^2 - (2/63)F^4$. We treat the charge transfer energy Δ as an adjustable parameter in our calculation. We fix the charge transfer energy at $\Delta = 2.76$ eV in order that the edge position of the RIXS intensity is consistent with the experiment. Note that the energy gap is determined by the charge transfer energy, since the electron system

Table I. Parameter values for the tight-binding model of La_2CuO_4 in units of eV. SK parameters are taken from ref. 28. $E_{e_g} - E_{t_{2g}}$ is the crystal field splitting between the Cu $3d$ e_g and t_{2g} states. $E_{\text{O}(1)}^p$ and $E_{\text{O}(2)}^p$ are the O $2p$ levels for the in-plane and apical oxygen, respectively. Slater Integral F^2 and F^4 are taken from ref. 30.

Cu	F^0	7.3, 11.3	F^2	11.41	F^4	7.308
	$E_{e_g} - E_{t_{2g}}$	1.18	Δ	2.71		
	$dd\sigma$	0.065	$dd\pi$	-0.067	$dd\delta$	-0.079
Cu-O(1)	$pd\sigma$	1.253	$pd\pi$	0.853		
Cu-O(2)	$pd\sigma$	0.568	$pd\pi$	0.377		
O(1)	$pp\sigma$	0.586	$pp\pi$	-0.384	$E_{\text{O}(1)}^p$	0
O(1)-O(2)	$pp\sigma$	-0.207	$pp\pi$	-0.196		
O(2)	$pp\sigma$	0.171	$pp\pi$	-0.025	$E_{\text{O}(2)}^p$	0.50

in La_2CuO_4 belongs to the charge transfer type insulator. We have checked that the RIXS spectra do not crucially depend on the values of F^0 . The parameters used in the calculation are listed in Table I.

2.2 Hartree-Fock approximation

Assuming the AFM ordering, we choose the unit cell that contains two Cu sites, one of which is a up spin site and another is a down spin site, and eight O sites, four of which are the in-plane O(1) sites and the others apical O(2) sites. Then we solve the Schrodinger equation $H\Psi = E\Psi$ by disregarding the fluctuation terms in H_I , i.e.,

$$H_I^{HF} = \frac{1}{2} \sum_i \sum_{\nu_1\nu_2\nu_3\nu_4} \Gamma^{(0)}(\nu_1\nu_2; \nu_3\nu_4) \langle d_{i\nu_2}^\dagger d_{i\nu_3} \rangle d_{i\nu_1}^\dagger d_{i\nu_4}, \quad (4)$$

where $\Gamma^{(0)}$ is the antisymmetric vertex function defined by

$$\Gamma^{(0)}(\nu_1\nu_2; \nu_3\nu_4) = g(\nu_1\nu_2; \nu_3\nu_4) - g(\nu_1\nu_2; \nu_4\nu_3), \quad (5)$$

with the bracket $\langle \dots \rangle$ indicating the ground state average.

For parameter values of F^0 , we take up two typical values $F^0 = 7.3$ and 11.3 eV, which correspond to the values of U used in refs. 32 and 20, respectively. For both cases, we obtain stable AFM solutions which have the energy gap $E_{\text{gap}} \sim 1.7$ eV and the spin moment at Cu site $s_{\text{Cu}} \sim 0.3\hbar$. The fact that the energy gap depends little on the F^0 values indicates that the system belongs to the charge transfer insulating phase. The density of states and the dispersion curves along some symmetric lines are shown in Figs. 2 and 3, respectively. The weight of the minority spin $x^2 - y^2$ states is indicated by the length of vertical bars in fig. 3. Labels assigned to the DOS peaks and to the dispersion curves will be related to the peaks in the RIXS intensities.

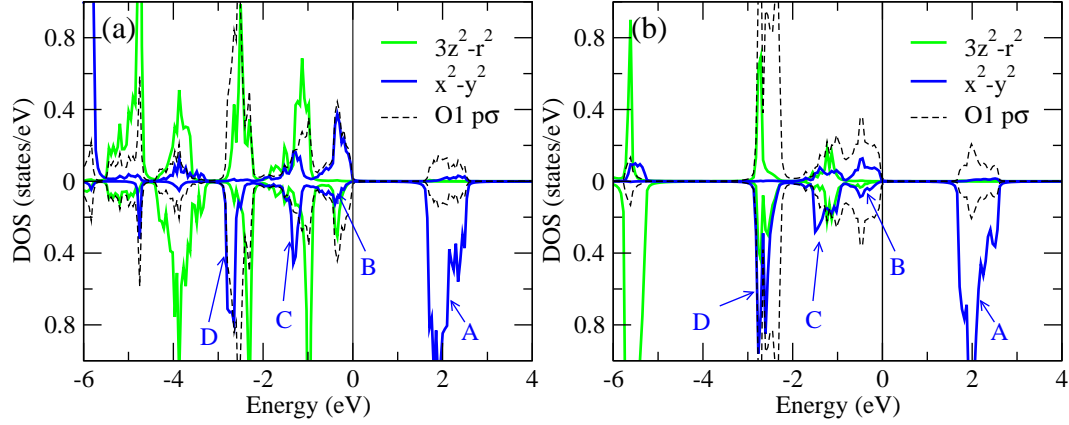


Fig. 2. (Color online) Density of states projected on the Cu $3d$ $x^2 - y^2$, $3z^2 - r^2$, and O(1) $2p$ σ states. The origin of energy is at the top of valence band. (a) and (b) are for $F^0 = 7.3$ and 11.3 eV, respectively.

The states in the conduction band (assigned A) consist mainly of the minority spin $x^2 - y^2$ state. Thereby the RIXS intensity is strongly correlated to the minority spin $x^2 - y^2$ state in the valence band, as discussed in the next section. The states around the top of valence band (assigned B) are mainly composed of the in-plane O $p\sigma$ states and the majority spin $x^2 - y^2$ states, but they also contain small weights of the minority spin $x^2 - y^2$ states, as seen from the figure. Their weights strongly depend on the momentum \mathbf{k} . Particularly, in the valence bands located just below the gap, the weight is negligible along the $(\pi/2, \pi/2)$ - $(\pi, 0)$ line, while it becomes discernible along the $(0, 0)$ - $(\pi/2, \pi/2)$ and $(\pi, 0)$ - $(0, 0)$ lines as denoted by B. The states labeled C and D noticeably contain the minority spin $x^2 - y^2$ states. We note that the states relating to the DOS peaks and the dispersion curves denoted by A, B, C, and D do not strongly depend on the F^0 values. The energy position and the weight of the $x^2 - y^2$ states are mainly controlled by the charge transfer energy Δ and the SK parameters. We also note that while the dispersion curves for the states denoted A and B are quite consistent with those calculated by the d - p model, it is difficult to find the correspondence for the other dispersion curves between the multiorbital model and the d - p model.

3. Formula for RIXS

We briefly summarize the NI formula for the RIXS, following ref. 26. In the RIXS process, the incident photon is absorbed by exciting a Cu $1s$ core electron to the unoccupied Cu $4p$ state, and a photon is emitted by recombining the $4p$ electron and the core hole. This process may be described by

$$H_x = w \sum_{\mathbf{q}\alpha} \frac{1}{\sqrt{2\omega_{\mathbf{q}}}} \sum_{i\eta\sigma} e_{\eta}^{(\alpha)} p_{i\eta\sigma}^{\dagger} s_{i\sigma} c_{\mathbf{q}\alpha} e^{i\mathbf{q}\cdot\mathbf{r}_i} + \text{H.c.}, \quad (6)$$

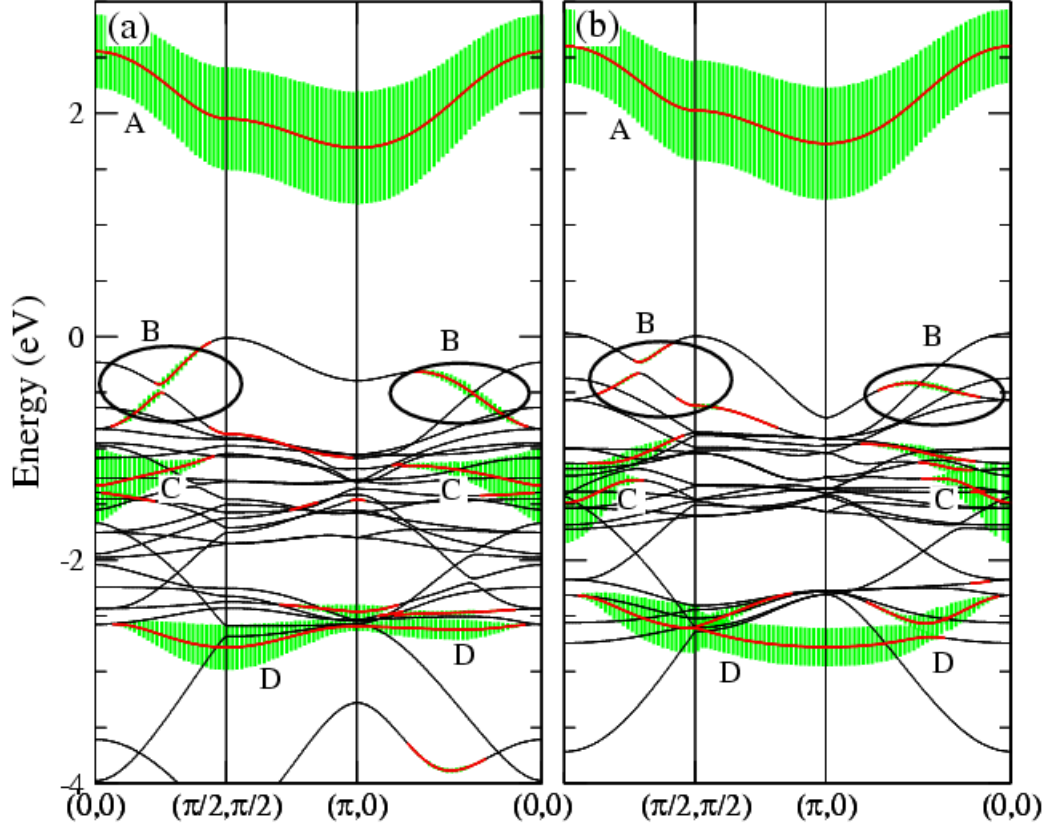


Fig. 3. (Color online) Dispersion curves along the several symmetric lines. The weight of minority spin $x^2 - y^2$ states is shown by the length of the vertical bar. The origin of energy is at the top of valence band. (a) and (b) are for $F^0 = 7.3$ and 11.3 eV, respectively.

where w represents the dipole transition matrix element between the $1s$ and the $4p$ states. We assume that w is constant, since it changes little in the energy range of 20 eV above the absorption edge. The $e_\eta^{(\alpha)}$ represents the η -th component ($\eta = x, y, z$) of two kinds of polarization vectors ($\alpha = 1, 2$) of photon. Annihilation operators $p'_{i\eta\sigma}$ and $s_{i\sigma}$ are for states $4p_\eta$ and state $1s$ at Cu site i , respectively. The annihilation operator $c_{\mathbf{q}\alpha}$ is for photon with momentum \mathbf{q} and polarization α . In the intermediate state of the RIXS process, the core-hole potential is acting on the $3d$ states, creating an electron-hole pair. The interaction is described by

$$H_{1s-3d} = V \sum_{i m \sigma \sigma'} d_{i m \sigma}^\dagger d_{i m \sigma} s_{i \sigma'}^\dagger s_{i \sigma'}, \quad (7)$$

where i runs over Cu sites. In the end of the process, an electron-hole pair is left with momentum and energy $q = (\mathbf{q}, \omega) = (\mathbf{q}_i - \mathbf{q}_f, \omega_i - \omega_f)$, where $q_i = (\mathbf{q}_i, \omega_i)$ and $q_f = (\mathbf{q}_f, \omega_f)$ are energy-momentum of incident and scattered photons.

The RIXS intensity is derived on the basis of the Keldysh-Green function scheme. The diagrammatical representation of the process is shown in Fig.4 (see ref.26 for details). Within

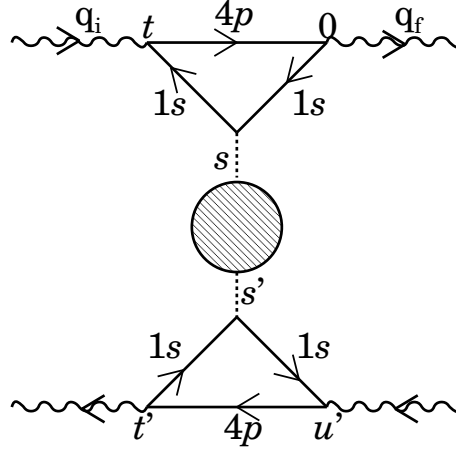


Fig. 4. Diagram for the RIXS intensity within the Born approximation for the 1s core-hole potential. The wavy lines represent photon Green's functions. The solid lines with the labels 4p and 1s represent the bare Green's functions for the 4p electron and the 1s core electron, respectively. The dotted lines represent the core-hole potential V . The shaded part represents the density-density correlation function of the Keldysh-type.

the Born approximation to the core-hole potential, we obtain

$$W(q_i, \alpha_i; q_f, \alpha_f) = \frac{N |w|^4}{4\omega_i \omega_f} Y_d^{+-}(q) \left| \sum_{\eta} e_{i\eta} L_B^{\eta}(\omega_i; \omega) e_{f\eta} \right|^2. \quad (8)$$

Here N is the number of unit cell, $e_{i\eta}$ ($e_{f\eta}$) is the η component of the polarization vector \mathbf{e}_i (\mathbf{e}_f) with $\eta = x, y, z$.

The factor $|\sum_{\eta} e_{i\eta} L_B^{\eta}(\omega_i; \omega) e_{f\eta}|^2$ describes the incident-photon dependence, which is given by

$$L_B^{\eta}(\omega_i; \omega) = \frac{V}{N} \int_{\epsilon_0}^{\infty} \frac{\rho_{4p}^{\eta\eta}(\epsilon) d\epsilon}{(\omega_i + \epsilon_{1s} + i\Gamma_{1s} - \epsilon)(\omega_i - \omega + \epsilon_{1s} + i\Gamma_{1s} - \epsilon)}. \quad (9)$$

The Γ_{1s} represents the life-time broadening width of the core-hole state, and ϵ_0 indicates the energy at the bottom of the 4p band. The $\rho_{4p}^{\eta\eta'}$ is the DOS matrix in the p symmetric states, which may be given by

$$\rho_{4p}^{\eta\eta'}(\epsilon) = \sum_{\sigma} \sum_{j\mathbf{k}} \phi_{\eta\sigma j}^*(\mathbf{k}) \phi_{\eta'\sigma j}(\mathbf{k}) \delta(\epsilon - \epsilon_j(\mathbf{k})), \quad (10)$$

where $\phi_{\eta j}(\mathbf{k})$ is the amplitude of the Cu p_{η} component in the band state specified by the band index j and momentum \mathbf{k} with eigenenergy $\epsilon_j(\mathbf{k})$. The off-diagonal components ($\eta \neq \eta'$) are negligible because of symmetry. This expression comes from the upper triangle in Fig.4.

The factor $Y_d^{+-}(q)$ in Eq. (8) is the density-density correlation function of the Keldysh type, which is defined by

$$Y_d^{+-}(\mathbf{q}, \omega) = \sum_{\lambda m \sigma} \sum_{\lambda' m' \sigma'} Y_{\lambda m \sigma, \lambda' m' \sigma'}^{+-}(q), \quad (11)$$

where

$$Y_{\lambda'm'\sigma',\lambda m\sigma}^{+-}(\mathbf{q}, \omega) = \int_{-\infty}^{\infty} \langle (\rho_{\mathbf{q}\lambda'm'\sigma'})^\dagger(\tau) \rho_{\mathbf{q}\lambda m\sigma}(0) \rangle e^{i\omega\tau} d\tau, \quad (12)$$

with

$$\rho_{\mathbf{q}\lambda m\sigma} = \sqrt{\frac{2}{N}} \sum_{\mathbf{k}} d_{\mathbf{k}+\mathbf{q}\lambda m\sigma}^\dagger d_{\mathbf{k}\lambda m\sigma}. \quad (13)$$

Here \mathbf{k} runs over the magnetic first BZ. The index $\lambda m\sigma$ specifies a tight-binding orbital at site λ with orbital m and spin σ . We assign $\lambda = 1, 2$ to two Cu sites in the unit cell.

Using the solution within the HFA, we obtain

$$Y_{\lambda m\sigma, \lambda' m' \sigma'}^{+-}(q) = \Pi_{\lambda m\sigma \lambda m\sigma, \lambda' m' \sigma' \lambda' m' \sigma'}^{+-}(q), \quad (14)$$

with

$$\begin{aligned} & \Pi_{\lambda_1 m_1 \sigma_1 \lambda_2 m_2 \sigma_2, \lambda'_1 m'_1 \sigma'_1 \lambda'_2 m'_2 \sigma'_2}^{+-}(q) \\ = & \frac{2\pi}{N} \sum_{\mathbf{k}} \sum_{j, j'} \delta(\omega - E_{j'}(\mathbf{k} + \mathbf{q}) + E_j(\mathbf{k})) [1 - n_{j'}(\mathbf{k} + \mathbf{q})] n_j(\mathbf{k}) \\ & \times \varphi_{\lambda_1 m_1 \sigma_1, j'}(\mathbf{k} + \mathbf{q}) \varphi_{\lambda'_1 m'_1 \sigma'_1, j'}^*(\mathbf{k} + \mathbf{q}) \varphi_{\lambda_2 m_2 \sigma_2, j}(\mathbf{k}) \varphi_{\lambda_2 m_2 \sigma_2, j}^*(\mathbf{k}). \end{aligned} \quad (15)$$

where $E_j(\mathbf{k})$ and $n_j(\mathbf{k})$ are the eigenenergy and the occupation number of the eigenstate specified by $j\mathbf{k}$, respectively. The $\varphi_{\lambda m\sigma, j}(\mathbf{k})$ represents the amplitude of the $3d$ orbital and spin $m\sigma$ at the Cu site λ in the energy eigenstate specified by $j\mathbf{k}$. This expression describes the excitation from occupied states to unoccupied states with Cu $3d$ amplitudes.

We treat the correlation effect on the electron-hole pair by the RPA. It is included into a vertex function:

$$Y_{\xi, \xi'}^{+-}(q) = \sum_{\xi_1 \xi_2} \sum_{\xi'_1 \xi'_2} \Lambda_{\xi_1 \xi_2, \xi}^*(q) \Pi_{\xi_1 \xi_2, \xi'_1 \xi'_2}^{+-}(q) \Lambda_{\xi'_1 \xi'_2, \xi'}(q). \quad (16)$$

with the vertex

$$\Lambda_{\xi_1 \xi_2, \xi}(q) = \left[\hat{I} - \hat{\Gamma} \hat{F}^{--}(q) \right]_{\xi_1 \xi_2, \xi \xi}^{-1}. \quad (17)$$

To simplify the notation, we abbreviate the indices $\lambda m\sigma$ as ξ . In Eq. (17), \hat{I} represents a unit matrix, and $\hat{\Gamma}$ is the bare four-point vertex given by

$$\left[\hat{\Gamma} \right]_{\xi_1 \xi_2, \xi_3 \xi_4} = \Gamma^{(0)}(m_1 \sigma_1 m_4 \sigma_4; m_2 \sigma_2 m_3 \sigma_3) \delta_{\lambda_1 \lambda_2} \delta_{\lambda_3 \lambda_4} \delta_{\lambda_1 \lambda_3}, \quad (18)$$

with $\xi_1 = \lambda_1 m_1 \sigma_1$, $\xi_2 = \lambda_2 m_2 \sigma_2$, $\xi_3 = \lambda_3 m_3 \sigma_3$, $\xi_4 = \lambda_4 m_4 \sigma_4$ ($\lambda_i = 1, 2$). Note that $\hat{\Gamma}$ is non-zero only for $\xi_1, \xi_2, \xi_3, \xi_4$ belonging to the *same* Cu site. The two-particle propagator $\hat{F}^{--}(q)$ is given by

$$\begin{aligned} \left[\hat{F}^{--}(q) \right]_{\xi_1 \xi_2, \xi_3 \xi_4} &= \frac{1}{N} \sum_{\mathbf{k}} \varphi_{\lambda_4 m_4 \sigma_4, j}(\mathbf{k}) \varphi_{\lambda_2 m_2 \sigma_2, j}^*(\mathbf{k}) \varphi_{\lambda_1 m_1 \sigma_1, j'}(\mathbf{k} + \mathbf{q}) \varphi_{\lambda_3 m_3 \sigma_3, j'}^*(\mathbf{k} + \mathbf{q}) \\ &\times \left[\frac{n_j(\mathbf{k}) [1 - n_{j'}(\mathbf{k} + \mathbf{q})]}{\omega - E_{j'}(\mathbf{k} + \mathbf{q}) + E_j(\mathbf{k}) + i\delta} - \frac{n_{j'}(\mathbf{k} + \mathbf{q}) [1 - n_j(\mathbf{k})]}{\omega - E_{j'}(\mathbf{k} + \mathbf{q}) + E_j(\mathbf{k}) - i\delta} \right] \end{aligned} \quad (19)$$

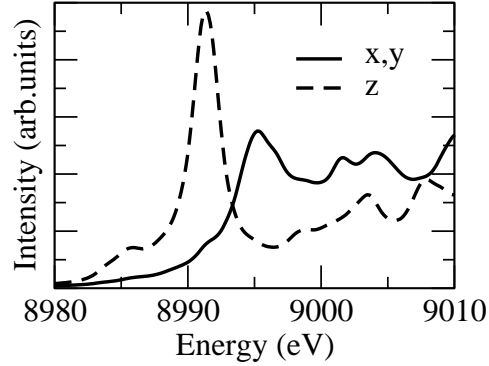


Fig. 5. The LDA $4p$ DOS convoluted by the Lorentzian function with FWHM $2\Gamma_{1s} = 1.6$ eV. In connection with the absorption coefficient, the origin of energy is shifted so that the prominent peak for the p_z DOS locates at 8991 eV. A thin line represents the absorption coefficient with taking account of the dipole matrix element evaluated by the band calculation.

For the details of the derivation, see refs.22 and 26. The RPA correction has been found to have an important role in the momentum dependence of the spectra.

4. Calculated Results

In order to calculate the incident-photon-dependent factor $|L_B^\eta(\omega_i; \omega)|^2$, we need the $4p$ DOS, $\rho_{4p}^{\eta\eta}(\epsilon)$. We evaluate the $4p$ DOS in a nonmagnetic (NM) phase on the basis of the muffin-tin KKR band structure calculation method within the LDA. It is known that the LDA fails to predict an insulating phase in the NM phase. However, the $3d$ states forming a metallic phase hybridize little with the $4p$ bands, giving rise to a minor effect on the $4p$ DOS distributing around 5-30 eV above the Fermi level. Figure 5 shows the $4p$ DOS convoluted with a Lorentzian function of FWHM $2\Gamma_{1s} = 1.6$ eV. Reflecting the layered structure, $\rho_{4p}^{zz}(\epsilon)$ is quite different from $\rho_{4p}^{xx}(\epsilon)$. Note that the $4p$ DOS is nearly proportional to the Cu K -edge absorption spectra under the condition that the dipole matrix element is constant and the interaction is neglected between the core hole and the $4p$ electron. In connection with the absorption coefficient, we set the energy difference between the Cu $1s$ level and the prominent peak in the $4p_z$ DOS to be 8991 eV.

Figure 6 shows the contour plot of $|L_B^\eta(\omega_i; \omega)|^2$ calculated by substituting the $4p$ DOS into Eq. (9). The enhancement starts earlier with increasing incident-photon energies in the out-of-plane polarization ($\eta = z$), reflecting the difference between $\rho_{4p}^{zz}(\epsilon)$ and $\rho_{4p}^{xx}(\epsilon)$. Except for these points, the general tendency of the enhancement factor looks similar in both polarizations; a large peak appears first in the small energy loss region and moves toward the higher energy loss region with increasing incident photon energy. The overall intensities decrease with increasing incident photon energy.

Another factor $Y_d^{+-}(q)$ mainly determines the RIXS spectra as a function of energy loss.

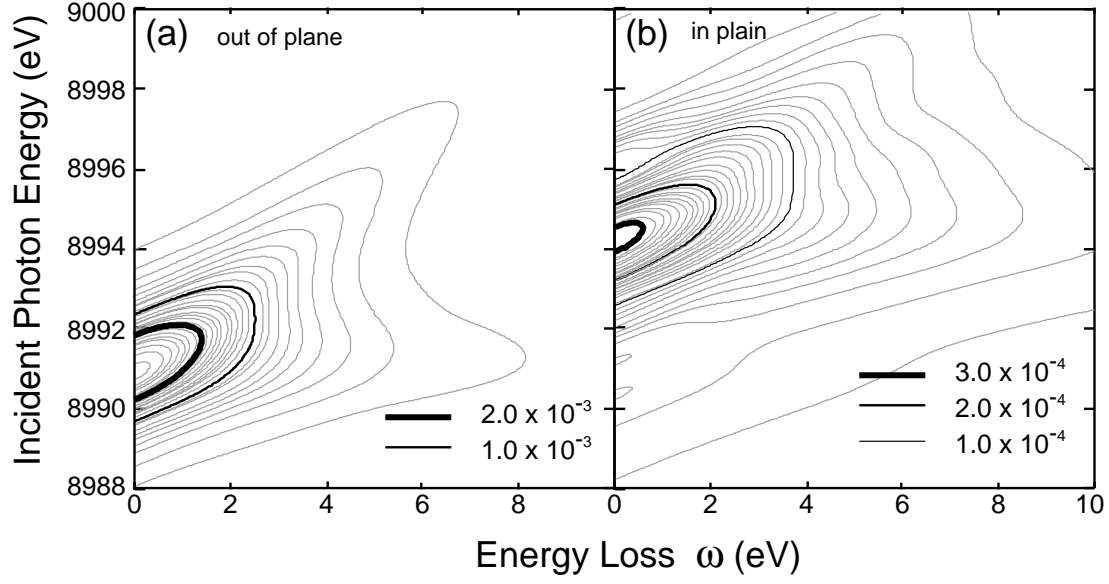


Fig. 6. Contour plot of $|L_B^\eta(\omega_i, \omega)|^2$ as a function of energy loss ω and incident photon energy ω_i in the out-of-plane polarization ($\eta = z$) (a) and in the in-plane polarization ($\eta = x$) (b) with $\Gamma_{1s} = 1$ eV. Units of the intensity are arbitrary.

We calculate this factor from Eqs. (14) and (16) with replacing the δ function by a Lorentzian function (FWHM = 0.2 eV) in order to simulate the instrumental resolution. Figure 7 shows the calculated results for \mathbf{q} along symmetry lines. We show the results with $F^0 = 11.3$ eV (corresponding to $U = 10.7$ eV in the d - p model analysis²⁰). We have checked that another choice $F^0 = 7.3$ eV leads to essentially the same result, except for the appearance of a weak intensity around $\omega = 6$ eV. We obtain continuous spectra ranging from $\omega = 2$ eV to 6 eV. Intensities around $\omega = 2$, 3.2, and 4.5 eV are caused by charge excitations of B \rightarrow A, C \rightarrow A, and D \rightarrow A transitions, respectively, within the $x^2 - y^2$ symmetry in the minority spin states (see Figs. 2 and 3).

We have a prominent peak around 4.5 eV, which stays at the same position with changing momentum. We also find that the spectral shape in the low energy region changes with changing momentum; a broad hump exists around $\omega = 2 - 4$ eV at $\mathbf{q} = (0, 0)$, which is enhanced by the RPA correction. This hump grows up to become a peak around 3.2 eV with changing \mathbf{q} along symmetry lines $(0, 0) - (\pi, 0)$ and $(0, 0) - (\pi/2, \pi/2)$. Meanwhile, the 3.2 eV peak is suppressed with changing \mathbf{q} along a symmetry line $(\pi/2, \pi/2) - (\pi, \pi)$, vanishing at $\mathbf{q} = (\pi, \pi)$. The RPA correction help suppress further the intensity in a region of $\omega = 2 - 4$ eV at $\mathbf{q} = (\pi, \pi)$, in contrast to the enhancement of the intensity at $\mathbf{q} = (0, 0)$.

The RIXS spectra are given by the product of $|L_B^\eta(\omega_i, \omega)|^2$ and $Y_d^{+-}(q)$. Figure 8 shows the calculated spectra as a function of energy loss ω in the out-of-plane polarization, in comparison with the experiments.^{13,15} At $\mathbf{q} = (0, 0)$, a hump-like intensity, which is found

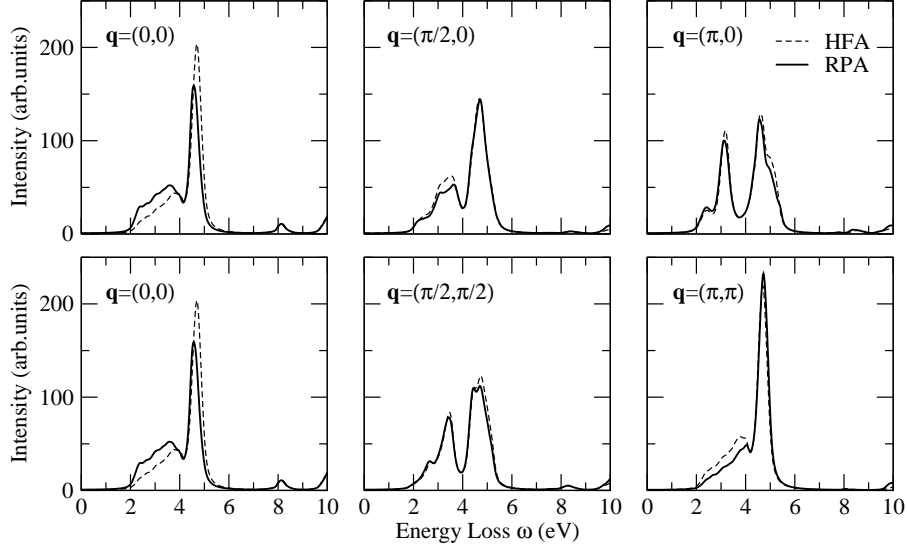


Fig. 7. The correlation function $Y_d^{+-}(\mathbf{q}, \omega)$ as a function of energy loss ω . Top panels are for \mathbf{q} along $(0, 0) - (\pi, 0)$, while bottom panels are for \mathbf{q} along $(0, 0) - (\pi, \pi)$.

around $\omega = 2 - 4$ eV in $Y_d^{+-}(\mathbf{q} = 0, \omega)$, is enhanced by $|L_B^z(\omega_i, \omega)|^2$ with $\omega_i = 8990 - 8994$ eV. Since the enhancement is larger with lower ω , intensities around $\omega = 2$ eV become a peak-like shape in the RIXS spectra. Intensities around $\omega = 3 - 4$ eV in $Y_d^{+-}(\mathbf{q} = 0, \omega)$ are moderately enhanced by $|L_B^z(\omega_i, \omega)|^2$, forming a very broad peak in the RIXS spectra. This broad spectral feature, which is not produced by the d - p model analysis,²⁰ is consistent with the experiments.¹³⁻¹⁵ The large 4.5 eV peak in $Y_d^{+-}(\mathbf{q} = 0, \omega)$ loses its weight in comparison with the intensities around $\omega = 2 - 4$ eV because of small enhancement by $|L_B^z(\omega_i; \omega)|^2$. With increasing $\omega_i (> 8994$ eV), the RIXS intensities around $\omega = 2 - 4$ eV decrease, since the peak in $|L_B^z(\omega_i; \omega)|^2$ as a function of energy loss ω moves to a region of higher ω . The intensity of the 4.5 eV peak first changes little and then decreases with further increasing ω_i , since the $|L_B^z(\omega_i, \omega)|^2$ becomes smaller. With changing \mathbf{q} along $(0, 0) - (\pi, 0)$, and $(0, 0) - (\pi/2, \pi/2)$, a peak develops around $\omega = 3.2$ eV in accordance with the development of the peak in $Y_d^{+-}(\mathbf{q}, \omega)$ for $\omega_i = 8992 - 8994$ eV. The intensity of the peak around $\omega = 3.2$ eV becomes comparable to the 4.5 eV peak at $\mathbf{q} = (\pi, 0)$ and $(\pi/2, \pi/2)$, while intensities in the region of $\omega < 3$ eV become smaller in comparison with the corresponding spectra at $\mathbf{q} = (0, 0)$. This behavior corresponds well to the experimental line shape at $\mathbf{q} = (\pi, 0)$, which looks like two peaks around $\omega = 3.2$ and 4.5 eV. With changing \mathbf{q} along $(\pi/2, \pi/2) - (\pi, \pi)$, intensities around $\omega = 2 - 4$ eV are suppressed by the RPA correction in accordance with the change of $Y_d^{+-}(\mathbf{q}, \omega)$, and only one peak is overwhelmingly left at 4.5 eV for a wide range of $\omega_i = 8990 - 8996$ eV. This explains the experimental spectra at $\mathbf{q} = (\pi, \pi)$, which looks like a single peak around $\omega = 4.5$ eV. Although the spectral shape is more consistent with the experiments¹³⁻¹⁵ than that calculated with the d - p model on the whole, several discrepancies between the present calculation and the

experiments still remain; the intensity around $\omega = 2$ eV is remarkably enhanced at $\mathbf{q} = (0, 0)$ with $\omega_i = 8990.5$ eV, the 4.5 eV peak is hardly discernible at $\mathbf{q} = (0, 0)$, the intensity at $\omega = 4$ eV is enough large forming a peak-like structure at $\mathbf{q} = (0, 0)$ with $\omega_i = 8992$ eV, and peak-like structures are found in the higher energy loss region $\omega \gtrsim 5$ eV in the experiments. We note that peak structures are observed around $\omega = 4.5$ eV at $\mathbf{q} \neq (0, 0)$, which seem to correspond well to the calculated 4.5 eV peaks. The calculated spectra at $\mathbf{q} = (0, 0)$ specifically fail to reproduce the observed spectral structure in $\omega = 4 - 4.5$ eV. To remove these discrepancies, we may need to take account of the electron correlations beyond the RPA and the effects beyond the Born approximation to the core-hole potential.

Figure 9 shows the calculated RIXS spectra as a function of energy loss ω in the in-plane polarization. The scale of the calculated intensity is the same as that in the out-of-plane polarization. The enhancement by $|L_B^x(\omega_i; \omega)|^2$ starts to be effective at ω_i about 3 eV higher with magnitude much smaller compared to that by $|L_B^z(\omega_i; \omega)|^2$. Reflecting these differences, the RIXS spectra are enhanced for $\omega_i > 8993$ eV with smaller intensities than those in the out-of-plane polarization. Except for these points, the change in spectra with changing \mathbf{q} and the incident-photon energy are similar to those in the out-of-plane polarization. This is consistent with the recent experiment by Kim et al.¹⁴

In comparison with our previous studies based on a d - p model with fixing ω_i at 8991 eV in the out-of-plane polarization,²² the spectral change obtained in the present paper with changing \mathbf{q} is consistent with our previous study. Difference is that the present study using a multiorbital tight-binding model leads to a distribution of intensities around 2 – 4 eV. This corresponds well to the experimental spectral shape. The present study also improves peak position from our previous value $\omega = 5.5$ eV^{20,22} to 4.5 eV, although the spectral shape still needs to be improved.

5. Concluding Remarks

We have analyzed the incident-photon-energy and polarization dependences on the RIXS spectra in La_2CuO_4 on the basis of the formula developed by Nomura and Igarashi. This formula expresses the RIXS spectra by a product of the density-density correlation function and the incident-photon dependent factor. To explain the fine structures found in the RIXS experiment, we have extended the d - p model used in our previous analyses to a multiorbital tight-binding model, which includes all the Cu $3d$ and O $2p$ orbitals as well as the full Coulomb interaction between $3d$ orbitals. We have calculated the density-density correlation function using the HFA and RPA, and the incident-photon-dependent factor using the $4p$ DOS from the ab initio band structure calculation. Fine structures are hardly reproduced by the d - p model. In the present detailed analysis, they are found in energy loss 2 ~ 5 eV, which vary with varying momentum and incident-photon energy, in semi-quantitative agreement with the experiment. Note that the peak shifts as a function of momentum should not be interpreted

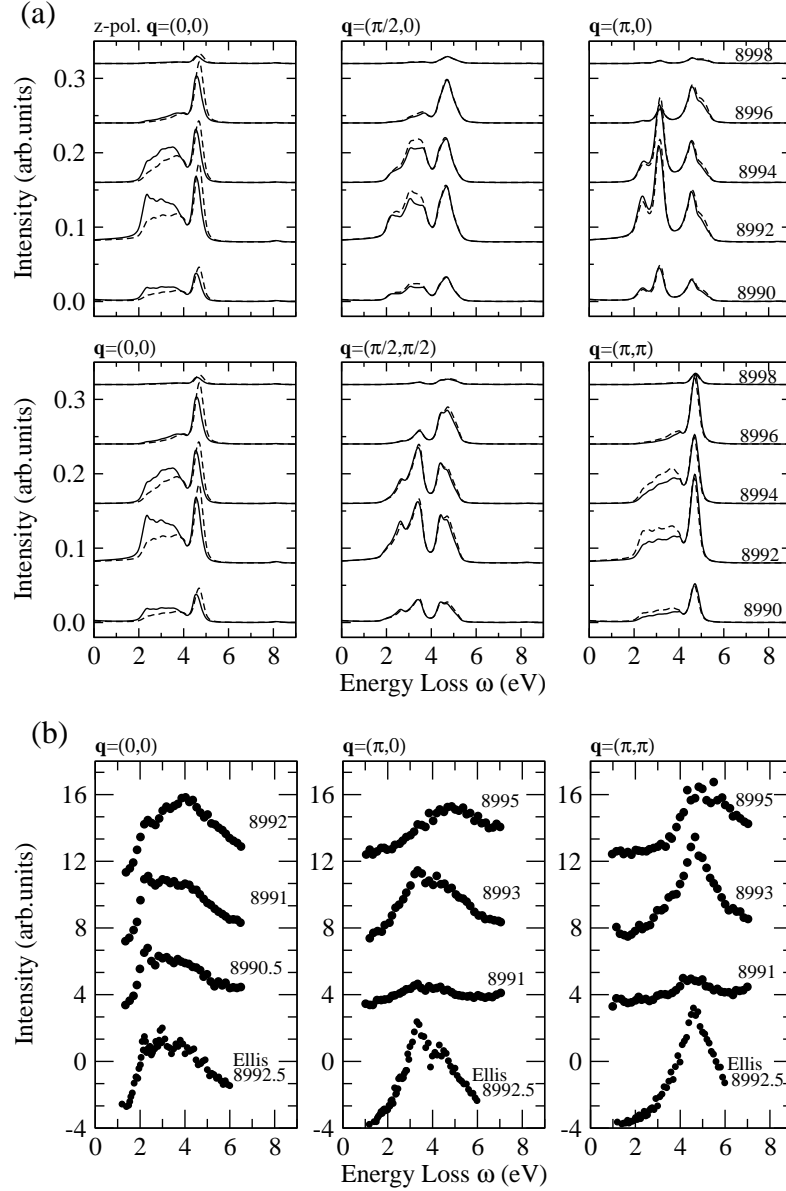


Fig. 8. (a) RIXS spectra as a function of energy loss in the out-of-plane (z) polarization. Top panels are for \mathbf{q} along a symmetric line $(0,0) - (\pi,0)$, while bottom panels are for \mathbf{q} along $(0,0) - (\pi,\pi)$. The solid and dashed curves are the spectra calculated within the RP and HF approximations, respectively. (b) RIXS spectra reproduced from refs. 13, 15. The curves denoted Ellis are taken from the ref. 15. The numbers in panels indicate the incident photon energy ω_i .

as a dispersion relation of a kind of exciton, because the peaks with broad widths constitute an energy continuum generated by a band-to-band transition. The experimental structures are not clear enough for more detailed comparison with the calculated spectra, we hope the correspondence will be clarified by improving the instrumental resolution.

The electron correlation works to modify the single-particle energy bands given by the

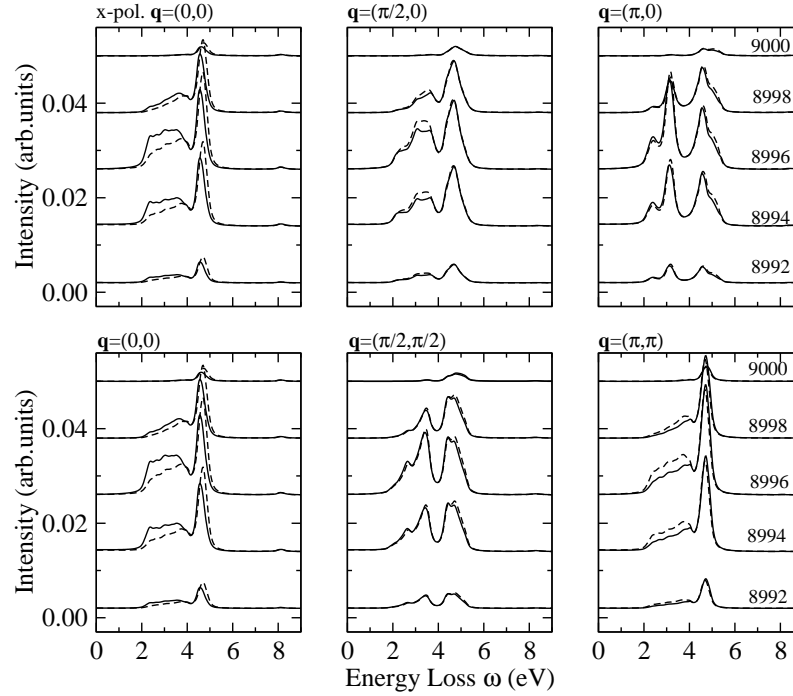


Fig. 9. RIXS spectra as a function of energy loss for the in-plane (xy) polarization. Each panel is for a typical \mathbf{q} value. The solid and dashed curves are the spectra calculated within the RP and HF approximations, respectively. The unit of intensity is the same as in Fig. 8.

HFA.³³ One prominent effect is a creation of "satellite" peak around 6 ~ 11 eV below the top of the valence band. According to the three-body scattering theory by the present authors,³⁴ the creation of satellite works to push the $3d$ states toward upper energy region in the valence band. Such modifications are not strong on the minority spin $x^2 - y^2$ states in the shallow energy region from the top of the valence band. Another effect is the reduction of the energy gap from the HFA value. We have taken account of this effect by adjusting the value of Δ to give the experimental energy gap within the HFA. Since the RIXS spectra for $\omega < 6$ eV come from the $3d$ states in the shallow energy region of the valence band, these points may explain why the HFA works rather well. As regards the Born approximation to the core-hole potential, our calculation explains semi-quantitatively the incident-photon energy dependence, indicating that the Born approximation works rather well. Although the present analysis is in semi-quantitative agreement with the experiment, several drawbacks remain as pointed out in the preceding section. Taking account of electron correlations and going beyond the Born approximation to the core-hole potential are desired for quantitative agreement with the experiment.¹³⁻¹⁵

Although experimental data have been accumulated for doped cuprates,¹⁰⁻¹² theoretical analyses are limited on a one-band Hubbard model within the exact diagonalization method,³⁵ and on a three-band Hubbard model analysis within the HFA on the basis of the present

formalism.³⁶ An analysis with a detailed model like the present paper may be necessary to clarify the momentum and incident-photon dependences of the spectra. Since electron correlations are expected to be more important in doped cuprates, such studies seem rather hard and are left in future.

Acknowledgment

We thank J. Mizuki for valuable discussions. This work was partially supported by a Grant-in-Aid for Scientific Research from the Ministry of Education, Culture, Sports, Science, and Technology, Japan.

References

- 1) J. Hill, C.-C. Kao, W. Caliebe, M. Matsubara, A. Kotani, J. Peng, and R. Greene: *Phys. Rev. Lett.* **80** (1998) 4976.
- 2) P. Abbamonte, C. A. Burns, E. D. Isaacs, P. M. Platzman, L. L. Miller, S. W. Cheong, and M. V. Klein: *Phys. Rev. Lett.* **83** (1999) 860.
- 3) M. Hasan, E. Isaacs, Z.-X. Shen, L. L. Miller, L. Tsutsui, T. Tohyama, and S. Maekawa: *Science* **288** (2000) 1811.
- 4) M. Z. Hasan, P. A. Montano, E. D. Isaacs, Z.-X. Shen, H. Eisaki, S. K. Sinha, Z. Islam, N. Motoyama, and S. Uchida: *Phys. Rev. Lett.* **88** (2002) 177403.
- 5) Y. J. Kim, J. P. Hill, C. A. Burns, S. Wakimoto, R. J. Birgeneau, D. Casa, T. Gog, and C. T. Venkataraman: *Phys. Rev. Lett.* **89** (2002) 177003.
- 6) T. Inami, T. Fukuda, J. Mizuki, S. Ishihara, H. Kondo, H. Nakao, T. Matsumura, K. Hirota, Y. Murakami, S. Maekawa, and Y. Endoh: *Phys. Rev. B* **67** (2003) 045108.
- 7) Y.-J. Kim, J. P. Hill, S. Komiya, Y. Ando, D. Casa, T. Gog, and C. T. Venkataraman: *Phys. Rev. B* **70** (2004) 094524.
- 8) Y.-J. Kim, J. P. Hill, H. Benthien, F. H. L. Essler, E. Jeckelmann, H. S. Choi, T. W. Noh, N. Motoyama, K. M. Kojima, S. Uchida, D. Casa, and T. Gog: *Phys. Rev. Lett.* **92** (2004) 137402.
- 9) S. Suga, S. Imada, A. Higashiya, A. Shigemoto, S. Kasai, M. Sing, H. Fujiwara, A. Sekiyama, A. Yamasaki, C. Kim, T. Nomura, J. Igarashi, M. Yabashi, and T. Ishikawa: *Phys. Rev. B* **72** (2005) 081101.
- 10) K. Ishii, K. Tsutsui, Y. Endoh, T. Tohyama, K. Kuzushita, T. Inami, K. Ohwada, S. Maekawa, T. Masui, S. Tajima, Y. Murakami, and J. Mizuki: *Phys. Rev. Lett.* **94** (2005) 187002.
- 11) K. Ishii, K. Tsutsui, Y. Endoh, T. Tohyama, S. Maekawa, M. Hoesch, K. Kuzushita, M. Tsubota, T. Inami, J. Mizuki, Y. Murakami, and K. Yamada: *Phys. Rev. Lett.* **94** (2005) 207003.
- 12) L. Lu, G. Chabot-Couture, X. Zhao, J. Hancock, N. Kaneko, O. Vajk, G. Yu, S. Grenier, Y.-J. Kim, D. Casa, and M. Greven: *Phys. Rev. Lett.* **95** (2005) 217003.
- 13) L. Lu, J. N. Hancock, G. Chabot-Couture, K. Ishii, O. P. Vajk, G. Yu, J. Mizuki, D. Casa, T. Gog, and M. Greven: *Phys. Rev. B* **74** (2006) 224509.
- 14) Y.-J. Kim, J. P. Hill, S. Wakimoto, R. J. Birgeneau, F. C. Chou, N. Motoyama, K. M. Kojima, S. Uchida, D. Casa, and T. Gog: *Phys. Rev. B* **76** (2007) 155116.
- 15) D.S. Ellis, J. P. Hill, S. Wakimoto, R. J. Birgeneau, D. Casa, T. Gog, Y.-J. Kim: *Phys. Rev. B* **77** (2008) 060501.
- 16) E. Collart, A. Shukla, J.-P. Rueff, P. Leininger, H. Ishii, I. Jarrige, Y. Q. Cai, S.-W. Cheong, and G. Dhalenne: *Phys. Rev. Lett.* **96** (2006) 157004.
- 17) K. Tsutsui, T. Tohyama, and S. Maekawa: *Phys. Rev. Lett.* **83** (1999) 3705.
- 18) K. Tsutsui, T. Tohyama, and S. Maekawa: *Phys. Rev. B* **61** (2000) 7180.
- 19) T. Nomura and J.-i. Igarashi: *J. Phys. Soc. Jpn.* **73** (2004) 1677.
- 20) T. Nomura and J.-i. Igarashi: *Phys. Rev. B* **71** (2005) 035110.
- 21) K. Okada and A. Kotani: *J. Phys. Soc. Jpn.* **75** (2006) 044702.
- 22) J.-i. Igarashi, T. Nomura, and M. Takahashi: *Phys. Rev. B* **74** (2006) 245122.
- 23) P. Nozières and E. Abrahams: *Phys. Rev. B* **10** (1974) 3099.
- 24) J. van den Brink and M. van Veenendaal: *Euro. Phys. Lett.* **73** (2006) 121.

- 25) P. Nozières and C. T. D. Dominicis: Phys. Rev. **178** (1969) 1097.
- 26) M. Takahashi, J. Igarashi, and T. Nomura: Phys. Rev. **75** (2007) 235113.
- 27) H. Ishii: private communication.
- 28) M. J. DeWeert, D. A. Papaconstantopoulos, and W. E. Pickett: Phys. Rev. B **39** (1989) 4235.
- 29) J. C. Slater and G. F. Koster: Phys. Rev. **94** (1954) 1498.
- 30) H. Eskes and G. A. Sawatzky: Phys. Rev. B **43** (1991) 119.
- 31) T. Mizokawa and A. Fujimori: Phys. Rev. B **53** (1996) 4201(R).
- 32) M. Takahashi, J. Igarashi, and P. Fulde: J. Phys. Soc. Jpn. **68** (1999) 2530.
- 33) M. Imada, A. Fujimori, and Y. Tokura: Rev. Mod. Phys. **70** (1998) 1039.
- 34) M. Takahashi and J.-i. Igarashi: Phys. Rev. B **54** (1996) 13566.
- 35) K. Tsutsui, T. Tohyama, and S. Maekawa: Phys. Rev. Lett. **91** (2003) 117001.
- 36) R. S. Markiewicz and A. Bansil: Phys. Rev. Lett. **96** (2006) 107005.